Zhang, W.; Kauer, M.; Halbherr, O.; Epp, K.; Guo, P.; Gonzalez, MI.; Xiao, DJ.... (2016). Ruthenium Metal–Organic Frameworks with Different Defect Types: Influence on Porosity, Sorption, and Catalytic Properties. Chemistry - A European Journal. 22(40):14297-14307. doi:10.1002/chem.201602641

Ruthenium Metal-Organic Frameworks with Different Defect Types: Influence on Porosity, Sorption and Catalytic Properties

Wenhua Zhang,[a] Max Kauer,[a] Olesia Halbherr,[a] Konstantin Epp,[b] Penghu Guo,[c] Miguel Gonzalez,[d] Dianne J. Xiao,[d] Christian Wiktor,[a] Francesc X. LIabrés i Xamena,[e] Christof Wöll,[f] Yuemin Wang,[f]* Martin Muhler,[c] and Roland A. Fischer*[b]

[a] Chair of Inorganic Chemistry II, Ruhr-University Bochum, Universitätsstrasse 150, 44801 Bochum (Germany)

[b] Chair of Inorganic Chemistry and Metal-Organic Chemistry, Technical University Munich, Lichtenbergstraße 4, D-85748 Garching (Germany), E-mail: roland.fischer@tum.de

[c] Laboratory of Industrial Chemistry, Ruhr-University Bochum (Germany), Universitätsstrasse 150, 44801 Bochum (Germany)

[d] Department of Chemistry, University of California, Berkeley, Berkeley 94720 California (USA)

[e] Instituto deTecnología Química (ITQ), Universidad Universitat Politécnica Politècnica de ValenciaValència, Consejo Superior de Investigaciones Científicas, Avenida de los Naranjos s/n, 46022 Valencia (Spain)

[f] Institute of Functional Interfaces (IFG), Karlsruhe Institute of Technology (KIT), Karlsruhe (Germany), E-mail: yuemin.wang@kit.edu

Abstract: Employing the mixed component, solid solution approach, various functionalized di-topic isophthalate (ip) defect generating linkers denoted as 5-X-ipH2, with X = OH (1), H (2), NH2 (3), Br (4) have been introduced into the mixed-valence ruthenium-analogue of [Cu3(btc)2] (HKUST-1) to yield Ru-DEMOFs (DE = “defect engineered”) of the general empirical formula [Ru3(btc)2-x(5-X-ip)xYy]n. The framework incorporation of 5-X-ip has been confirmed by a number of techniques including PXRD, FT-IR, UHV-IR, TGA, 1H-NMR, N2 sorption as well as XANES. Interestingly, Ru-DEMOF (1c) with 32% framework incorporation of 5-OH-ip reveals the highest BET surface area (1300 m2/g, N2 adsorption, 77K) among all samples (including the parent framework [Ru3(btc)2Yy]n). The characterization data are consistent with two kinds of structural defects induced by 5-X-ip framework incorporation: type A, modified paddlewheel nodes featuring reduced ruthenium sites (Ru+, 0<δ<2) and type B: missing nodes leading to enhanced porosity. Their relative abundances depend on the choice of the functional group X in the defect linkers. The defects A and B appeared also to play a key role in sorption of small molecules (i.e., CO2, CO, H2) as well for the catalytic properties of the samples (i.e., ethylene dimerization and Paal-Knorr reaction).

Introduction

Metal-organic frameworks (MOFs), constructed from metal ion nodes and organic linkers, have been studied in a number of fields including gas sorption[1], gas separation,[2] catalysis,[3] sensing,[4] drug delivery.[5] Recently, it has been recognized that MOFs, similar to other (crystalline) solid-state materials, are typically not perfect crystals with infinite periodic repetition or ordering of the identical groups of atoms in space. In fact, defects of various types and length scales (even more generally: structural heterogeneity) cannot be rigorously avoided during the synthesis and crystal growth and often play an important role for the material properties.[6] The diversity of MOF structures connected with the issues of intrinsic and

intentional structural defects, non stoichiometry and heterogeneity suggests a much broader approach for understanding and tailoring their chemical and physical properties.[7] Ravon and co-workers reported Zn-MOFs featuring defects as acid active catalytic centers (generated through fast precipitation or partial linker substitution) that are responsible for shape selectivity in alkylation of large aromatics molecules.[8] Vermoortele et al. demonstrated generation of defects in UiO-66(Zr) via the coordination modulation approach.[9] As a result, better catalytic performance in several Lewis-acid catalyzed reactions was observed for the "defect engineered" MOF. Recently, a direct correlation was found to exist between the concentration of missing linker defects in UiO-66 and its catalytic activity for the acid-catalyzed esterification of levulinic acid with alcohols. [Ref] Controlled introduction and characterization of specific defects into MOFs is quite a challenge including the comparison with the parent (more or less) "defect-free" reference samples.

[Cu3(btc)2]n (also known as HKUST-1)[10] as well as the isostructural family [M3(btc)2]n (M = Mo,[11] Cr,[11b, 12] Ni,[11b, 13] Ru,[11b, 14] Zn,[11b, 15], btc = benzene-1,3,5-tricarboxylate) attract considerable attention over last years, mainly due to coordinatively unsaturated metal-sites (M-CUS), which could be readily available after appropriate post-synthetic treatment. Intentional defect generation in [Cu3(btc)2]n was initially reported by Baiker et al. who studied partial replacing of the btc by the homologous pyridine-3,5-dicarboxylate (pydc) linker and revealed enhanced catalytic activity of the modified MOF in the oxidation of benzene derivatives related to modified coordinatively unsaturated sites (M-CUS) at the nodes.[16] Subsequently, we have demonstrated that not only pydc, but also a series of other defect generating linkers can be framework incorporated in case of [Cu3(btc)2]n.[17] Interestingly, functionalized mesopores along with the M-CUS appeared to be generated in such defect-engineered MOFs (DEMOFs). In parallel, Hupp et al. gave an account of the enhanced porosity by introducing isophthalate (ip) into [Cu3(btc)2]n.[18] The concept of defects engineering by a mixed component approach using fragmented linkers together with the parent one was also expanded to the isostructural Ru-analog.[19] Ru-DEMOFs [Ru3(btc)2-x(pydc)xYy]n (Y = counter-ion, Cl-, OH-, OAc, etc.; $0 < y \leq 1.5$) were obtained through direct mixing of H2pydc and H3btc in one-step solvothermal synthesis. The generation of reduced Ruδ+ ($0<\delta<2$) sites at the paddlewheel nodes as a consequence of defect linker incorporation was correlated with enhanced CO uptake as well as improved catalytic activity in olefin hydrogenation. Remarkably, low temperature (100 K) dissociative chemisorption of CO2 leading to coordinated CO was observed by UHV-FTIR spectroscopy in the dark. However, regardless of obviously more advanced properties as compared with the parent material, the actual compositions of these Ru-DEMOFs are very difficult to establish and are not entirely clear. This stems from the structural complexity of such multi-component solid solution MOFs and a range of possible compositional variations need to be taken into account which are not mutually exclusive (counter-ions, residual synthesis components such as linkers, coordination modulators etc.).

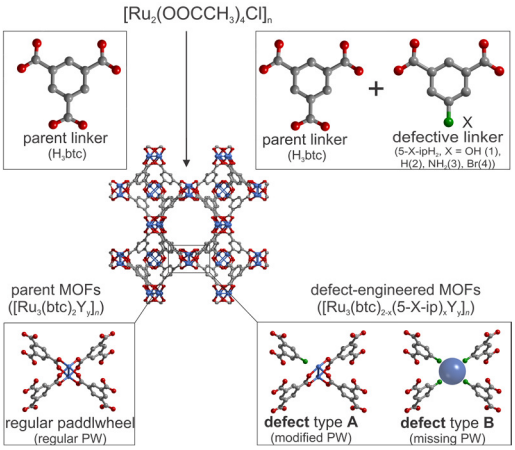

Figure 1. Design concept of the Ru-DEMOFs applying the mixed component/fragmented linker solid solution approach and sketch of the two possible, most important paddlewheel-node related defects.

Figure 1 summarizes the concept of defects introduction into mixed-valence [Ru3(btc)2Yy]n by using divalent isophthalate linkers as fragmented variants of trivalent btc. Mainly, two types of defects need to be distinguished here. Type A refers to structurally and electronically modified paddlewheel units (missing one carboxylate ligator function), in which (at least) one out of the four bridging carboxyl groups from the parent btc linker in the regular paddlewheels has been partly substituted by the (neutral) functional group of the defect linker. Consequently, for charge compensation, the metal sites could be either partly reduced (mixed-valence state) or may carry additional anionic (mono-valent) ligands (Y)[7, 19] However, apart from such type A, defects of type B could be formed, where whole paddlewheel nodes are eliminated from the structure, as it has been demonstrated in the case of ip introduction into [Cu3(btc)2]n.[18] It is conceivable, that such missing node defects could be formed in a correlated fashion during the MOF crystal growth process and in such a case larger areas of missing nodes may be generated to yield mesopores. Being mainly studied in Cu-HKUST-1, a comprehensive understanding of the nature and formation of different types of isolated local and larger scale correlated defect sites in DEMOFs of the [M3(btc)2]n family and MOFs in general is very limited and this research is still at its infancy.[7] Herein we follow-up our previous investigations on defects engineering in [Ru3(btc)2Yy]n using H2pydc as (single) defect generating linker.[8b] Similar to our previous more elaborate study on defect engineered Cu-HKUST-1[17] we now selected a series of 5-X-isophthalic acids (5-X-ipH2, X = OH, H, NH2, Br) and mixed then with H3btc to yield the Ru-DEMOFs of the general formula [Ru3(btc)2-x(5-X-ip)xYy]n (Figure 1). A number of complementary characterization methods were applied to obtain compositional and microstructure data of the materials. The aim was to at least qualitatively assess the tendency of type A and type B defect formation as a function of synthetic conditions and the chosen 5-X-ip linker. Several catalytic reactions, such as ethylene dimerization and Paal-Knorr reaction (usually running under Lewis acidic conditions) as well as low temperature CO2→CO dissociative chemisorption in the dark under UHV conditions, have been chosen as test reactions to monitor the influence of defects on the performance of the Ru-DEMOFs.

Results and Discussion

In the following we give a comprehensive account on the conducted experiments, obtained analytical and characterization data for elucidation of the defect structure of Ru-DEMOFs of the general formula [Ru3(btc)2-x(5-X-ip)xYy]n. The main goal of our presented study is to

substantiate the hypothesis of type A and type B defect formation in these systems as introduced above (Figure 1). Due to the amount of collected information on the systems only the most significant data have been selected for display in Figures and Tables in the main text in order to save space for concise discussion. Most of the systematic data documentation is moved to the supporting information.

Synthesis and characterization of the Ru-DEMOF materials (1a-d, 2a-d, 3a-d, 4a-c)

All Ru-DEMOF samples were obtained according to the previously published procedure,[8b] using [Ru2(OOCCH3)4Cl]n, H3btc and defect generating 5-X-ipH2 as starting materials in the water/acetic acid solution under solvothermal conditions. The sample numbering scheme is based on the framework incorporated 5-X-ip linker: X= OH (1), H (2), NH2 (3) or Br (4). Further labeling (a, b, c etc.) refers to various levels (molar %) of defect linker incorporation. The PXRD patterns of the as-synthesized and activated samples indicate that all materials (except 2d) are crystalline and isostructural with the parent Ru-MOF that is obtained employing the same method just employing H3btc, only. (Figures S1 and S2). It should be noted that Ru2+/3+ ions may be prone to reduction to eventually yield Ru metal during solvothermal synthesis, depending on the conditions. However, reflections at the 2θ range of 40-45° were not found in all PXRD patterns of both the as-synthesized and activated samples, thus suggesting absence of a significant amount of Ru-nanoparticles (Ru-NPs). Reflections at 42.1° and 44° are usually assigned to (001) and (101) faces of hexagonal close-packed metallic Ru-particles or Ru-NPs.[20] Further characterizations, XANES in particular, which are described below provide additional indication for the absence of Ru/RuOx-NPs in the obtained Ru-DEMOFs.

Regardless 2d, thermal gravimetric analysis (TGA) shows no decomposition of the prepared materials before 250 °C, suggesting that thermal stability of Ru-DEMOFs is preserved as compared to the parent MOF (Figure S3). The incorporation and quantification of defect linkers have been initially testified by NMR spectroscopy of the digested samples after activation and the assessment of porosity (Table S2). Thus, in the 1H-NMR spectra of the samples 1a-d appearance of two additional peaks (compared with the parent Ru-MOF) at 7.51 ppm and 7.89 ppm is clearly seen (Figure S4). These two resonances could be attributed to the aromatic protons of 5-OH-ip linker. Expectedly, upon increasing feeding amount of the defect linker (5-OH-ipH2), the intensities of its characteristic resonances also increases in the digested sample solution (Figure S4). The same was observed also for the samples with ip defect linker (series 2a-c). Resonances corresponding to the protons of ip are seen at 8.4 ppm, 8.1 ppm and 7.6 ppm (Figure S5). The framework incorporation amount of ip in 2a-c increases upon the rise of defect linker feeding. However, the incorporated ip amount was found to be higher than expected from the H3btc : H2ip feeding ratio rather than staying the same or a little less. This result might be attributed to the slightly different coordination equilibria that correlate with the Brønsted acid dissociation constants of the used linkers: pKa (H3btc) = 3.12, 3.89, 4.70 and pKa (H2ip) = 3.46, 4.46.[21] However, the pKa differences are small and a conclusive explanation based on pKa is not straightforward. Dincă et al. argued that deprotonated btc could serve as a counter-ion to provide the charge balance of [Ru2]5+ units in Ru-analog of Cu-HKUST-1.[11b] Our investigations concluded that H3btc could reside in the pores of [Ru3(btc)2Yy]n rather than as deprotonated counter-ions.[22] Both studies indicated that the linker used for the synthesis can still be present in the obtained materials. Hence, it is conceivable that the defect generating H2ip linker can also reside either as a counter-ion or as guest molecule in the pores of the Ru-DEMOFs (2a and 2b). Therefore, the amount of incorporated ip has been found higher than the feeding ratio of H2ip

: H3btc. Indeed, very weak IR-bands in the range of ν(C=O), ν(C=C) or νas(COO) vibrations (1736-1521 cm-1) have been observed in case of samples 2a-2d. However, the close position of the ν(C=O) bands of non-coordinated acetic acid (1715-1640 cm-1),[23] protonated/non-coordinated H2ip (1670 cm-1) and H3btc (1680 cm-1) (see Figure S8) makes it hard to unambiguously determine the exact origin of these weak vibrations.

Here it should be pointed out that in our current study in 1H-NMR spectra of all digested Ru-DEMOF samples the resonance at ca. 1.91 ppm originated from the –CH3 groups of acetate has been detected. To emphasize, in our previous investigations on the parent single-linker Ru-MOFs obtained from various Ru-precursors and the Ru-DEMOFs with pydc defect linker the same resonance due to acetate in the digested samples was always observed as well.[19, 22] We anticipate three main origins of the presence of acetate in the discussed Ru-MOFs: i) it may act as a counter-ion to compensate the overall charge of the framework (Figure S7a); ii) owing to the competition with btc and 5-X-ip, it could be residual / non-substituted and paddle wheel coordinated acetate-groups of the used Ru-precursor ([Ru2(OOCCH3)2Cl]n) (Figure S7b); iii) finally, it might reside as AcOH in the pores of the framework through weak interactions and, therefore, cannot be easily removed by washing and subsequent thermal activation (i.e., heating at 150 °C under dynamic vacuum). To recall, the glacial acetic acid / water mixture (AcOH : H2O = 19 : 1) was found to be essential for a successful synthesis and was always used for all reported Ru-(DE)MOFs (see Experimental Section). Besides, employed linkers may also serve as guest molecules as has been mentioned above. Attempts to evaluate the presence of acetic acid and linkers from the IR spectra is not quite feasible due to the overlapping of the bands of νas(COO) and νs(COO) (coordinated in a bidentate-bridging mode and free-coordinated carboxylate group)[24] as well as low intensity of the respective bands. Consequently, the presence of acetate (mainly) and non-reacted free linkers used in Ru-DEMOFs raises questions about the actual sample compositions and local structures and, thus, causes more complications with ambiguous interpretation of the analytical data than in case of the homologous Cu-DEMOFs.[17] The compositions of the Ru-DEMOFs samples discussed in this work have been derived by taking into account the whole experimental results and a full account on is given in the Supporting Information (Tables S3 and S4). Due to not sufficiently quantitative digestibility of the samples 3a-d, detection and determination of the defect linker contents (5-NH2-ip) from 1H-NMR measurements was not possible. Nevertheless, the IR spectra of these samples provide a qualitative evidence for the 5-NH2-ip incorporation. Indeed, the observed bands at 1651 cm-1 and 1264 cm-1 stem from δ(N-H) and ν(C-N) vibrations of the 5-NH2-ip (Figure S8). In case of the 5-Br-ip (samples 4a-c), the gradual increase of intensities of the respective signals in both 1H-NMR and TEM-EDX spectra suggests the presence of defect linker in these Ru-DEMOFs (see Figures S6 and S9).

To support further the framework incorporation of the defect linker and rule out its extra framework inclusion within the pores in a high quantity, N2 sorption measurements for the activated samples have been carried out. The N2 sorption isotherms at 77 K for all samples (1a-d, 2a-d, 3a-d and 4a-c) reveal type I isotherm without any hysteresis loop (Figure S10), indicating that all Ru-DEMOFs are microporous materials.[25] In general, while comparing with the Brunauer-Emmett-Teller (BET) surface area (SBET) of the parent Ru-MOF (998 m2/g), one can consider Ru-DEMOFs being analogous. In other words, the considerably high SBET of the discussed Ru-DEMOFs rules out substantial guests occlusion and pore blocking such as by non-reacted defect linkers, acetate or Ru/RuOx-NPs. Interestingly, when 5-OH-ipH2 is used as defect linker, SBET of the Ru-DEMOFs gradually increases until 5-OH-ip is incorporated up to 32% (1c) (Figure 2). Notably, the SBET of this sample 1c is the highest among all [Ru3(L)2Yy]n isostructural

MOFs (including the single-linker and other mixed-linker Ru-DEMOFs reported so far).[14a, 19] This indicates that the 5-OH-ip is a good candidate for the defects engineering in the Ru-MOFs. To remark, for the comparison of the obtained SBET values for Ru-MOFs with the homologous Cu-MOFs it might be more informative using m2/mmol units (due to substantial difference in the molecular weight of Cu and Ru). Thus, as could be seen from the Table S6, the SBET of the parent Ru-MOF (964 m2/mmol) is quite similar to that one of a typical reference sample [Cu3(btc)2]n (1049 m2/mmol). More importantly, the SBET of the Ru-DEMOF solids slightly increases in comparison with both parent analogs.

In contrast with the Ru-DEMOFs series 1, when H2ip defect linker has been employed, the samples 2a-2d exhibit in general lower porosity. However, the SBET of the samples 2a and 2b are still higher than SBET of the parent Ru-MOF. Nonetheless, upon increase of the ip contents the surface area decreases. Thus, considering porosity characteristics, the optimum incorporation extent of defect linker in these series stays at 28% (sample 2b, 20% feeding). In case of 5-NH2-ip defect linker, the porosity of the 3a-c Ru-DEMOFs is fully maintained, while increasing of the feeding level to 50% leads to porosity decrease instead (sample 3d, SBET = 781 m2/g). These observations in 2a-d and 3a-d series are probably due to the accommodation of unreacted 5-X-ipH2 in the pores. Along with the increasing feeding of 5-X-ipH2 the competition between btc and 5-X-ip increases. Subsequently, it is more difficult to rule out the presence of unreacted 5-X-ipH2 as the reason of the decreasing SBET. In the same line of reasoning, the SBET of the samples 4a-c dramatically decreased from 996 to 693 m2/g. Hence, the optimized incorporation of 5-Br-ip can only reach up to 17% (4a). Notably, in our previously studies on the defect-engineered Cu-HKUST-1 generation of mesopores was observed.[17] Curiously, in present case of the homologous Ru-DEMOFs we notice an opposite trend, that might be attributed to the preference of isolated defects rather than to the correlated defects in the framework (Figure S11).

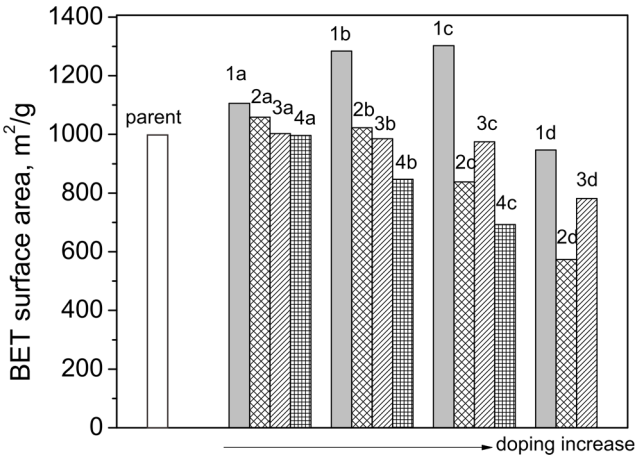

Figure 2. The variation of the BET surface area (SBET) derived based on measured N2 sorption isotherms (77 K) upon increase of the defect linker doping. 'Parent' stands here for parent single-linker Ru-MOF (with only btc). In the samples 1a-1d 5-OH-ip serves as a defect linker; 2a-2c – ip; 3a-3d – 5-NH2-ip; 4a-4c – 5-Br-ip, respectively.

XANES, XPS and UHV-FTIR studies: ruthenium oxidation state variation as indication of defect type formation

As earlier mentioned, in our previous studies on doping of the Ru-MOF with defect pydc linker, we have assigned the introduced local defects, according to Baiker et al.,[16] as modified Ru-paddlewheels with three coordinating btc and one pydc linker in which the pyridyl-N site acts as a weakly binding ligator-site over the Ru-dimer. Such structural irregularities are associated with (partly) missing linker function (i.e., carboxylate) and consequently steric and electronic modification of the Ru-SBUs (see Figure 1). Additionally, partial ruthenium reduction has been observed. Namely, apart from the expected Ru2+ and Ru3+ (as in the parent Ru-MOF) we revealed also distinctly reduced framework Ru-species (Ruδ+, 0<δ<2) in the pydc-doped Ru-DEMOFs.[19] Since pydc is a divalent (anionic) linker of one charge less than btc, charge compensation by reduction of some Ru-ions may take place (in the absence or in parallel of other charge compensating effects such as accommodating additional Y anions). Note, we reported also the significant formation of mixed-valence Cu2+/Cu1+ paddlewheels for the related pydc-doped Cu-HKUST-1 material.[17] Interestingly, in parallel studies on isostructural Cu-HKUST-1 doped with ip (rather than pydc and other 5-X-ip) predominantly defects B (see Figure 1) and no significant change of the copper oxidation state were reported.[18] Thus, the choice of the defect generating linker in combination with type of the metal and the synthetic conditions (doping level) most likely defines the types of defects induced in the particular type of MOF structure. Therefore, we were interested to investigate the oxidation state of the Ru-centers in the series with 5-X-ip defect linkers (X = OH, H, NH2 and Br) in comparison with our previous data on the pydc-case,[19] and supporting the assignment of the defect types.

Initially, XANES studies have been performed. XANES spectra (Figure S12) show deviation of the pre-edge jump derivative for the samples 1a-d from that one of the parent Ru-MOF. For 1a-c, the position of pre-edge jump is gradually shifted to the lower energy, suggesting reduced Ru-sites with oxidation states lower than 2+ or 3+. This is assigned to the generation of defects A in the samples 1a-c. However, the position of the pre-edge jump in case of the sample 1d turned again to the higher energy, illustrating that the amount of the reduced Ru-species is now decreased with respect to the 1a-c. The different tendency suggests that the defects B may also be created when 5-OH-ip linker was framework incorporated in a quantity higher than 32%. The same trend has been observed for the 5-NH2-ip linker (samples 3a-c). Indeed, the XANES spectra of the samples 3a-b suggest again the presence of the reduced Ruδ+ (0<δ<2) sites, but the oxidation state of Ru-centre in 3c is the same as in the parent Ru-MOF (Figure S14). Furthermore, when the 5-Br-ipH2 defect linker is employed, the oxidation state of Ru is varied as well (in particular sample 4a, Figure S15). These data support the assignment of locally modified node defects A for these samples. Interestingly, the position of the pre-edge jump in case of the ip-doped samples 2a-b does not change compared with that in the parent Ru-MOF (Figure S13). The Ru oxidation state is not affected by the incorporation of the ip, which could be taken as indication of predominant defects B for 2a-b. When the functional group of the defect linkers changes from small, coordinative inert H to the somewhat larger and coordinative more suitable ligator-sites like -OH, -NH2 or -Br, the defects A are favored in case of relatively low doping level. However, upon rising the doping level defects B are increasingly created along with some remaining defects A, resulting in less pronounced variation of the oxidation state of Ru in the defect engineered samples compared with the parent material.

It is important to note, that the curve of XANES spectra (normalized absorption vs. energy, Figure S16) of the all Ru-DEMOFs samples as well as the parent Ru-MOF are strikingly different from those measured for the Ru-NPs, metallic Ru and RuO2. These observations support PXRD results (see above and Figures S1 and S2, SI) and allow also to rule out the presence of other Ru-phases as significant impurities in the Ru-DEMOFs including parent Ru-MOF.[20] Thus, we assume that

it is valid to assign all Ru-species to the metal-nodes of the frameworks. Further information on the local environment of Ru can be obtained also from EXAFS, however, the fitting of the experimental data with various models of Ru-DEMOFs requires abundant time to work on it, which is one of our directions in the future.

High-resolution X-ray photoelectron spectroscopic (XPS) studies have been subsequently carried out to confirm the assignments based on XANES and for a more quantitative estimation of the relative abundance of the different Ru-species (Ru3+, Ru2+ and Ruδ+) in the Ru-DEMOFs. The samples 1a, 1c, 1d, 2a and 2b with 5-OH-ip and ip defect linkers, respectively, have been selected. Remarkably, similar to the related pydc-doped Ru-DEMOFs we elaborated earlier,[19] reduced Ruδ+-species have been found in the Ru-DEMOFs (samples 1a, 1c and 1d) in addition to the Ru2+- and Ru3+-species. Two Ru 3d doublets (3d5/2 and 3d3/2) at ca. 281.6 and 285.8 eV as well as at 282.6 and 286.8 eV attributed to the Ru2+- and Ru3+-species, respectively, are seen in the deconvoluted XP spectra of all measured samples (Figure 3). In addition, another Ru 3d doublet appears at ca. 280.5 and 284.7 eV in the Ru-DEMOFs samples 1a, 1c and 1d.

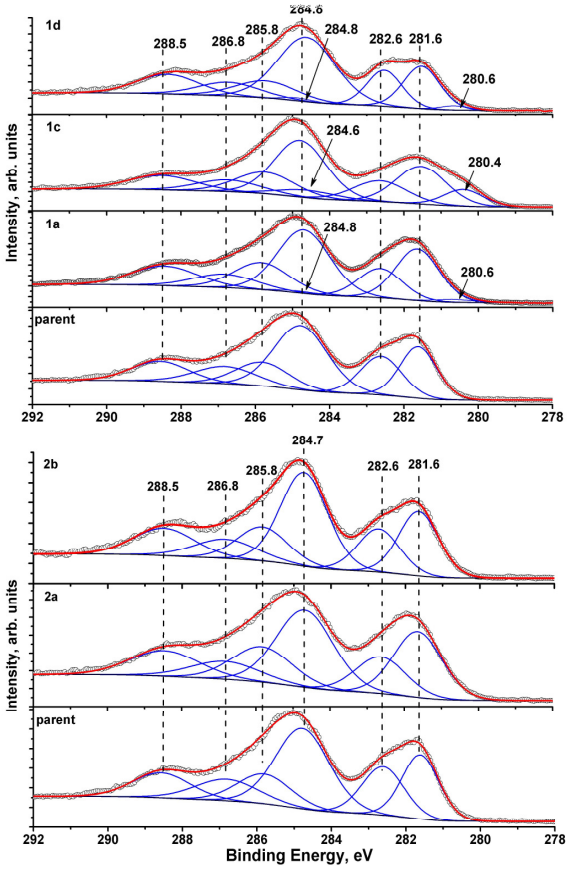

Figure 3. Deconvoluted XP spectra of the Ru-DEMOFs samples 1a (8% of 5-OH-ip), 1c (32% of 5-OH-ip), 1d (37% of 5-OH-ip), 2a (15% of ip) and 2b (28% of ip) in Ru 3d and C 1s regions in comparison with parent Ru-MOF.

On the basis of quantitative estimations of the XPS spectra, some variation of the Ru3+/Ru2+ ratio and, in particular, reduction to Ruδ+ in 1a, 1c and 1d can be clearly seen (Table S6). From the parent Ru-MOF to the Ru-DEMOF sample 1a, the ratio of Ru3+ / Ru2+/ Ruδ+ varies from 1 / 1.24 / 0 to 1 / 1.75 / 0.08, indicating that the incorporation of defect linker induces partial ruthenium reduction (i.e., relative concentrations of the Ru2+ and Ruδ+ increase). Moreover,

upon increasing the incorporation level of 5-OH-ip to 32 % for 1c (feeding level 30%), the amount of the reduced Ruδ+-species considerably increases to the highest value (Ru3+ / Ru2+/ Ruδ+ = 1 / 1.69 / 0.59) among the all studied samples. Importantly, the Ruδ+-related doublet decreases significantly in intensity with further slight increase of the incorporation to 37% for 1d (feeding level 50 %). This is in contrast to the observation for pydc-doped Ru-DEMOFs, where a continuous rise of the Ruδ+ signals was detected along with increasing degree of pydc2- incorporation.[19] The relatively lower concentration of Ru2+ and Ruδ+ in 1d (Ru3+ / Ru2+/ Ruδ+ = 1 / 1.23 / 0.09), as compared to the respective ratios estimated for 1c, can be explained by our assumption of simultaneous generation of both defects A and B with distinct preference of B over A at higher feeding concentrations of 5-OH-ip. Interestingly, for the ip-doped samples 2a-b no highly reduced Ru□+ have been observed in the XP spectra (no Ru3d doublets at ca. 280.5 and 284.7 eV; Figure 3). These data confirm the assignment deduced from XANES data suggesting that application of defect linker with the coordinatively inactive functional group H (2a-b) is likely to more selectively induce missing node defects B in the Ru-DEMOFs without Ru reduction (as this is indicative for a type A defect). According to the results of XANES and XPS, we thus conclude that the Ru-DEMOFs materials with 5-X-ip (X= OH, NH2 and Br) contain predominantly defects of type A, especially at moderate incorporation levels. However, the simultaneous generation of defects B in these samples is also likely as indirectly deduced from the non-linear dependence of the XANES and XPS data on the doping level.

Consequently, UHV-IR spectroscopic investigations employing CO as a probe molecule have been carried out on two representative samples 1c and 1d to gain complementary evidence on the valence states of framework Ru sites and the associated defect types. Parent Ru-MOF was reported to reveal bands at 2172 and 2127 cm-1 arising from CO interactions with Ru3+ and Ru2+, respectively (Figure S18).[19] Apart from these two bands, the spectra of the samples 1c and 1d show additional bands at 2041 and 1998 cm-1, which can be attributed to CO bound to reduced Ruδ+ (0<δ<2) and again indicate the presence of defects A (i.e., modified paddlewheels). Notably, the relative intensity of the band at 2171 cm-1 (Ru3+) decreases largely as compared to the parent Ru-MOF, which is associated with the generation of reduced Ru2+/□+ species. On the other hand, increasing the doping of 5-OH-ip from 32% (1c) to 37% (1d) leads to a significant attenuation of the CO bands associated with Ru2+ (ca. 2127 cm-1) and Ruδ+ (ca. 2041 and 1998 cm-1), whereas for pydc-doped Ru-DEMOFs the abundance of reduced Ruδ+ increases gradually upon increasing the amount of pydc.[19]. These findings confirm again the coexistence of defects A and B in Ru-DEMOFs at relatively high degree of 5-OH-ip incorporation (1d). The formation of defect B, namely missing Ru-paddlewheels, is accompanied by lowering the abundance of Ru2+ and Ruδ+ metal centers in the framework, which explains the observed changes of the decreased intensity of Ru2+ and Ruδ+ in the sample 1d.

In our earlier report on pydc-doped Ru-DEMOFs we communicated on the low temperature CO2→CO dissociative chemisorption under UHV conditions in the dark environment, a feature which is not inherent for the parent Ru-MOF.[19] It was concluded, that the CO2→CO reduction might be triggered by the reduced Ruδ+- sites and the pyridyl N-sites in the proximity of the modified Ru-centers at the nodes. In order to confirm these assumptions further, we have studied the same reaction at Ru-DEMOFs that feature reduced Ruδ+-sites. As these sites have been created by the incorporation of the 5-OH-ip linker in 1a-1d, we have selected two representative samples, 1c and 1d, both exhibiting high 5-OH-ip incorporation but quite different levels of Ru2+ and Ru□+. As shown in Figure 4, upon CO2 dosing for both the parent Ru-MOF and Ru-DEMOFs 1c an intense and broad IR band appears at 2336 cm-1 that is assigned to the asymmetric stretching mode □as(CO2) of physisorbed CO2 binding linearly at various Ru-

sites.[14b] The weak band at 2273 cm-1 indicates the presence of a minority CO2 species originating probably from the adsorption of a small amount of 13CO2 with an expected isotopic shift of 1.03. Apart from the CO2-related bands, two other bands at 2041 cm-1 and 1993 cm-1 have been observed in 1c, that are assigned to vibrations of CO bound to the reduced Ruδ+-sites, matching our previous data on pydc-doped Ru-DEMOF.[19] This result indicates dissociative chemisorption of CO2 to CO (reduction) in Ru-DEMOF with 5-OH-ip defect linker (1c), whereas the parent Ru-MOF is essentially inactive. However, in comparison to the extremely high reactivity of pydc-doped Ru-DEMOFs in which CO2 is nearly totally converted to CO at higher concentrations of pydc defective linker (e.g. 30%),[19] the production of CO is rather limited for 5-OH-ip doped Ru-DEMOFs (Figure 4). Interestingly, Ru-DEMOF 1d, is almost inactive for CO2 dissociation (Figure S19). We correlate this observation to the much less Ru□□□and in turn to the more significant formation of missing node defects (type B) for 1d as compared to 1c. Overall, the presented IR data demonstrate that the 5-OH-ip doped Ru-DEMOF samples show much less reactivity for CO2 activation as compared to pydc doped samples. This cannot be attributed only to the relatively low concentration of reduced Ru□□□□ In our previous study,[19] we suggested the CO2 activation being promoted by pydc2- linker due to the presence of basic pyridyl N sites in proximity to the reactive Ru□□□□This hypothesis is indirectly supported by the properties of samples 1c and 1d.

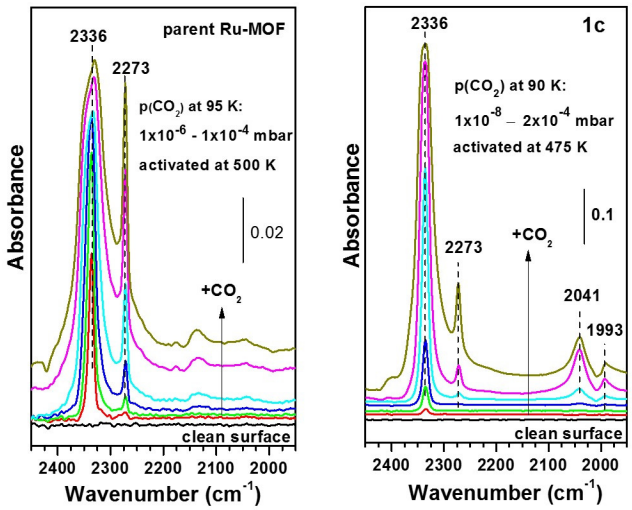

Figure 4. UHV-IR spectra of 1c (right) compared with parent Ru-MOF (left) upon CO2 dosing at 90-95 K after annealing the sample at 475-500 K. The bands at 2041 cm-1 and 1993 cm-1 are assigned to vibrations of CO bound to reduced Ruδ+-sites and indicate dissociative chemisorption of CO2.

The combined spectroscopic characterization data (XANES, XPS, UHV-FTIR with CO and CO2 as probes) presented above suggest more or less consistent, however complicated picture on the abundance of the two kinds of defects. Overall we assume both types A and B being simultaneously generated in the Ru-DEMOFs in the case of coordinative weakly binding ligator-sites at the fragmented linkers. Type A appears to be favored at low incorporation levels, e.g. 1a (8%) and becomes more abundant up to a certain threshold, e.g. 1c (32%). Along with a further increase of incorporation level, e.g. 1d (37%), defects of type B appear to dominate over type A. One should be aware that the possibility of formation and distribution of various defect types is rather diverse and may not be restrict to those mentioned here (see other possible defects and a summary of possible defect combinations in Table S8 and Figure S20, SI). Additional

characterization information and quantitative determination of the defect types requires additional work including support by the theoretical modeling.

CO2, CO and H2 sorption properties of Ru-DEMOFs

The previous characterizations suggest the existence of two types of defects (A and B) being present in the samples in different absolute and relative amounts as a consequence of the 5-X-ip framework incorporation. Both are likely to influence the gas sorption properties of the Ru-DEMOFs. Hence, we studied the adsorption of CO2, CO and H2 at range of samples. In general, the results obtained and discussed in the following are not very conclusive as the observed changes in gas uptake as a function of defect linker of incorporation are small or even close to the error of the measurements. Nevertheless, we present the data and provide a tentative discussion with respect to the possibly counter acting effects of the two types of defects in the samples.

CO2 adsorption isotherms (298K) of the parent reference sample Ru-MOF and 1a and 1c display a gradual enhancement of the adsorption capacity in the order Ru-MOF < 1a < 1c along with rising incorporation degree of the defect linker (Figure S21). However, the CO2 uptake of the sample 1d revealed to be 2.9 mmol/g at 1 bar, and lies within the order Ru-MOF < 1d < 1c (Table S9). According to our studies on different defects in the series 1a-1d, these results are not unexpected. The increase of the CO2 uptake is attributed to the reduced Ru-sites at the type A defects and somewhat lowered uptake of 1d is attributed to less abundant Ru-sites as a consequence of missing metal-nodes (i.e., type B defects). Hence, higher incorporation level of the defect linker in the sample 1d does not promote the increase of the CO2 uptake.

Furthermore, CO adsorption of the parent Ru-MOF, 1a and 1c at 298 K also illustrates the tendency of enhanced uptake in case of the Ru-DEMOF samples (Figure S22). The small difference between the sample 1a and the parent Ru-MOF on CO adsorption is attributed to the low incorporation degree of the 5-OH-ip defect linker (8%). Along with the increase of the defect linker incorporation (such as in 1c), the CO uptake rises even at very low pressure (ca. 4 mbar). This increase of the CO capacity of the Ru-DEMOF is probably due to the generation of the modified paddlewheels of type A, which expose more open sites as one carboxylate ligator-site of btc is substituted by the hydroxyl-group of 5-OH-ip. Besides, the electronic density is varied as the oxidation state of ruthenium at the CUS is changed. Both could contribute to the enhancement of the adsorption properties.

The H2 (at 77K) adsorption isotherms of the parent Ru-MOF and the Ru-DEMOFs 1a and 1c follow nearly the same trend as in case of CO2 and CO adsorption (Figure S23a). Both defects engineered materials 1a and 1c exhibit higher H2 uptake at 1 bar than the parent intact framework. However, H2 capacity is slightly lower when the incorporation of 5-OH-ip is more than 8%, as in case of 1c and 1d. This could be due to the more significant generation of the type B defects in these Ru-DEMOFs. The calculated isosteric heats of adsorption (–Qst) reveal an order with 1c > 1a > parent Ru-MOF when comparing the respective values at 1 mmol (H2) / Ru2-paddlewheel (what might be considered as the saturation adsorption of H2 at the regular paddlewheel) (Figure S23b). This suggests stronger binding affinity of H2 for Ru-DEMOF with 32% of incorporated 5-OH-ip (sample 1c), what again is attributed to the relative higher amount of Ruδ+-sites in 1c.

Moving further to the 5-NH2-ip defect linker, respective Ru-DEMOFs (3a-3c) display the same tendencies in their absorption behavior of CO2 and H2 as in their SBET (N2). From the results of the XANES studies we have already revealed that defects B are likely to be generated at lower doping levels 3a-c (5-NH2-ip) as compared to the samples 1a-d (5-OH-ip). This difference in defect A/B abundance leads to variation of the CO2 and H2 adsorption in case of the 3a-c series. Even though 3a-c display higher uptake of CO2 and H2 than the parent Ru-MOF, the uptake of CO2 and H2 does not further increase after the feeding level of 5-NH2-ip is raised above 10% (3a) (Figures S26 and S27). Similar to 1d, we assign the decrease of the uptake of CO2 and H2 at 1 bar observed for 3c as compared with 3a-b to more abundant type B defects.

Another indication of the suggested counter acting effects of the defect sites is the comparison of the CO2 and H2 uptakes at 2a, 2b and 4a with the parent Ru-MOF (Figures S24, S25, S28 and S29). However, the variations are too small to be regarded as significant and will be not discussed here.

Catalytic test reactions

1. Ethylene dimerization

Ethylene dimerization utilizing MOF supported catalysts has recently attracted a lot of attention due to its modifiable characteristic under molecular level.[26] Most of the reported MOF catalysts bear isolated single-metal (e.g., Ni, Ir) active-sites. Ru-MOF materials as heterogeneous catalysts for the ethylene dimerization have not been studied yet, although chemisorbed Ru-complex on de-aluminated zeolite Y and Ru-complex itself catalyzing ethylene to butene have been already reported.[27] It is known that the redox activity of Rh in RhCa-X Zeolite plays an important role on catalyzing ethylene dimerization.[28] Having distinct Ru-CUS available in the Ru-DEMOFs (i.e., different Run+-species being potentially involved into the redox-process(es) of the reaction flow), 1a (8% of 5-OH-ip) and 1c (32% of 5-OH-ip) samples have been selected for testing them as catalysts in the selected test reaction. In addition, parent Ru-MOF has been used as a reference. Thus, activated Ru-DEMOFs were loaded into a reactor to catalyze ethylene dimerization in toluene at different temperatures under the pressure of 800 psi (≈ 55 bar). In general, all reactions led to the formation of butene without producing any other α-olefins (Tables S10). Addition of Et2AlCl as co-catalyst accelerates the conversion (Table S10, entry 2 vs. entry 3). When the reaction has been conducted at 26 °C, lower yield has been obtained compared to those at 80 °C (Table S10, entry 4 vs. entry 5). However, reactions conducted for 1h and 24h give almost the same TOF (0.88 vs. 0.92 h-1), suggesting that the Ru-DEMOF 1c does not suffer the deactivation as a function of on-stream time. Therefore, parent Ru-MOF and Ru-DEMOFs 1a and 1c have been employed to study the dimerization of ethylene in toluene under optimized condition (800 psi, 80 °C, 2h) in the presence of Et2AlCl. The obtained product was analyzed by gas chromatography. As we can see from the entry 5-7 in the Table S10 and Figure 5, the TOF value of 1a and 1c increase along with increase of the incorporation level of defect linker in comparison with the parent Ru-MOF. Since the contents of the reduced Ruδ+-sites in 1c is the highest among 1a-d series (according to our study above), there should be more M-CUSs in 1c and therefore it affords the chance to enhance the catalytic activity in the reaction. Indeed, the transformation of ethylene to butene is the highest (TOF = 4.36 h-1) when employing 1c as a catalyst. This value is still much lower than that using zeolite supported Ru-complex catalyst in the presence of H2 (4.36 vs. 216 h-1). However, it is higher than the TOF value (1 × 10-4 s-1 = 0.36 h-1) in the reported reaction without the presence of H2 .[27b] Distinction

between butene isomers, optimization of the reaction conditions using Ru-DEMOF materials (such as usage of H2) as well as clarifying the mechanism of this reaction are currently under investigation. Nevertheless, the preliminary results give a rather clear hint that obtained Ru-materials could be utilized as catalyst for the dimerization of ethylene. Due to the diverse modification of MOF materials themselves our current investigations on the ethylene dimerization using Ru-DEMOFs can afford a platform for the further studies on MOFs catalyzing in this field .

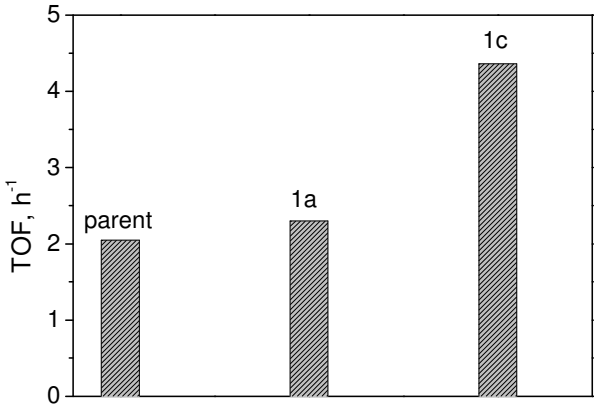

Figure 5. The tendency of TOF value for parent Ru-MOF and Ru-DEMOF samples 1a and 1c utilized as catalysts for transformation of ethylene into toluene (800 psi, 80 °C, 2h) in the presence of Et2AlCl (0.81 ml, 1M in heptane). TOF (turnover frequency) = mol product / (mol Metal (catalyst)*h).

2. Paal-Knorr reaction

Paal-Knorr pyrrole synthesis has attracted great attention due to the huge synthetic variety of pyrroles and their derivatives which are key intermediates for various pharmaceutical drugs.[29] The reaction is typically run under protic or Lewis acidic conditions, using primary amines and diketones. As we know from earlier reports, parent Ru-MOF ([Ru3(btc)2Y1.5]n) is constructed from Ru2-paddlewheels, in which the axial Ru-positions are partly occupied by strongly binding Y or by other weakly guest molecules. After thermal treatment a fraction of the axial positions can be exposed as open Lewis acidic sites (useful as catalytic site, for instance). With regard to the structure of the Ru-DEMOFs discussed in this contribution, two kinds of defects are present. The modified paddlewheel units (A) could provide the materials with additional sites around the partly reduced Ru-centers. On the other hand, the eliminated entire Ru-paddlewheel clusters (B) can form vacant-sites to play a role on affecting the adsorption properties, especially when the functional X-group at the defect generating linker is as small as H. Hence, Ru-DEMOFs 1a-1c, 2a and 2b have been utilized for catalyzing the reaction of 2,5-hexadione and phenylamine in toluene at 90 °C to form dimethyl-phenyl-1H-pyrrole (Scheme 1).

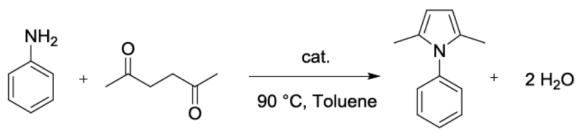

Scheme 1. The Paal-Knorr catalytic reaction.

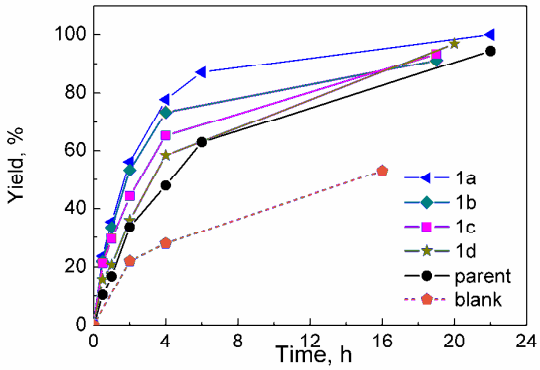

Figure 6. Time-yield plot of Paal-Knorr synthesis of phenylamine reacting with 2,5-hexadione, giving the pyrrole employing Ru-DEMOFs 1a-1d (with 8%, 20%, 32% and 37% 5-OH-ip incorporation, respectively) as catalysts in comparison with the parent Ru-MOF(parent). Blank stands for the experiment where on catalyst was added into the reaction mixture.

It is interesting to note that all of the selected Ru-DEMOFs show apparently enhanced conversion of phenylamine to the pyrrole within the initial 4 hours in comparison with the parent Ru-MOF (Figure 6). All the samples tested were found to be stable under reaction conditions, as confirmed by comparing the PXRD of fresh and used materials. Among the used materials, Ru-DEMOFs 1a and 2a exhibit the highest catalytic activity, although the other Ru-DEMOFs (1b, 1c, 1d and 2b) incorporate more defect linker (Table S11). The steric hindrances and distinct defect types (A vs. B) could be the main reason of this phenomenon. When Ru-DEMOF samples with 5-OH-ip defect linker (1a-d) were employed as catalysts, the yield of pyrrole has been increased from 48% (using parent Ru-MOF as the catalyst) to 58% (1d), 65% (1c), 73% (1b) and 77% (1a), respectively. This is assigned to the presence of the reduced Ru-centers (defects of type A) in these materials. Reduced, softer binding Ruδ+-sites can be more easily coordinated to the O atom of the carbonyl group, which favors the nucleophilic attack from the lone-pair of the amino group of phenylamine. However, when the incorporation of 5-OH-ip increases the gradual dominance of the defects B in these materials probably eliminates part of the reactive metal-centers, thus, affecting the catalytic activity of the 1b-d samples. On the other hand, Ru-DEMOF 2a displays higher yield of pyrrole compared to the parent Ru-MOF (82% vs. 48%) regardless of the partial absence of the metal-centers (defects B) (Figure S30). This could be a result of the smaller steric hindrance surrounding the Ru-CUSs while employing the H2ip defect linker. When the contents of the incorporated defect linker are rather small (i.e., as in 2a), the negative influence caused by missing metal centers is relatively insignificant compared with the positive effect of the smaller steric hindrance. Therefore, 2a Ru-MOF material shows as high catalytic activity in present reaction as 1a. Similar observations have been found for the samples 1b-c because of somewhat larger steric hindrance of OH-groups in spite of the type A defect in these materials.

Conclusions

Applying the solid solution approach a range of Ru-DEMOFs ([Ru3(btc)2-x(5-X-ip)xYy]n) isostructural to HKUST-1 were obtained with the framework incorporated defect linkers 5-OH-ip (1a-d), ip (2a and 2b), 5-NH2-ip (3a-c) and 5-Br-ip (4a)). Comparably high SBET have been measured for Ru-DEMOF samples (947-1302 m2/g), when considering the parent Ru-MOF material [Ru3(btc)2Y1.5]n (704-998 m2/g).[14a, 22] The highest level of defect linker

incorporation appeared to be 37% (1d, 5-OH-ip). The data are consistent with two kinds of defects (A and B) being introduced to the Ru-DEMOFs depending on the nature of the functional groups (X) of the defect linkers (5-X-ip; see Figure 1). Defect linkers with steric less demanding X-groups of probably still existing but weaker coordinative binding properties as a carboxylate ligator are likely to favor type A defects, defined as modified paddlewheel nodes exhibiting reduced Ru□+-sites. Along with the increasing of the defect linker contents, defects of type B, i.e. missing node defects, can be created simultaneously in the DEMOFs. When the functional groups in the defect linker 5-X-ip are much smaller than carboxylate and non-coordinating X (such as H), the defects of type B, defined as missing node defects, apparently become more dominant even in case of low doping level (case of 2a and 2b). The more or less simultaneous presence of two kinds of defects leads to the synergetic and as well counteracting effects on the porosity, sorption and catalytic properties. In fact, Ru-DEMOF 1c (32% 5-OH-ip incorporation), in which defects of type A are more dominant, reveals the highest BET surface area (1302 m2/g) among the all samples, including parent Ru-MOF and its DEMOF derivatives reported so far.[19] Concerning the enhanced gas sorption properties, type A defects are more important than those effects related to the defects of type B, as reduced and more accessible Ruδ+-sites have been produced in the type A. When it comes to the catalytic activity, Ruδ+-sites in Ru-DEMOF 1c are suggested to be responsible for the significant increase of TOF value of ethylene dimerization, as clearly seen while comparing with the parent Ru-MOF and 1a in which no or less Ruδ+-sites are present. However, in case of Paal-Knorr pyrrole reaction, the possible steric hindrance between the functional groups (OH) at the defect linker and 2,5-hexadione substrate is suggested to be responsible for the reduced activity of the Ru-DEMOFs 1a-d, although they all feature enhanced conversion compared with the parent Ru-MOF. All in all, the described Ru-DEMOFs obtained via solid solution approach employing various defect linkers turned out to be rather complex materials to be studied and characterized. Nevertheless, the observed spectroscopic evidences as well as effects on sorption properties and catalytic performance reasonably fit into a model of the two types of defects, modified and missing nodes (see Figure 1), respectively.

Experimental Section

Materials. Ruthenium SBU precursor [Ru2(OOCCH3)4Cl]n[30] as well as the parent single-linker Ru-MOF[14] were prepared following procedures previously described in the literature. All other reagents were available commercially and used without further purification. Before further manipulations, all activated samples were stored in a glove-box under inert Ar atmosphere.

Methods. The Powder X-Ray diffraction (PXRD) data for all the as-synthesized samples and activated samples (2a-2d, 4a-4c) were performed on an X' Pert PRO PANalytical equipment (Bragg–Brentano geometry with automatical divergence slits, position sensitive detector, continuous mode, room temperature, Cu-Kα radiation, Ni-filter, in the range of 2θ = 5–50°, step size 0.01°). Activated sample were prepared on a silicon wafer in an Ar-filled glovebox right before the measurement starts. For the measurement of activated samples (Ru-DEMOFs series 1 and 3), the data were collected at beam line BL9 of the synchrotron radiation facility DELTA at a wavelength of 0.4592 Å using a two-dimensional MAR345 image plate detector. The sample was filled into standard capillaries (0.5-mm diameter) in an Ar-filled glovebox and measured. The data were integrated using the program package Fit2D[31] and transformed to the CuKα radiation (λ = 1.54178 Å) used for all other PXRD measurements on reported materials for the convenient comparison. Elemental Analyses data were obtained from the Mikroanalytisches

Laboratorium Kolbe in Mülheim an der Ruhr (http://www.mikro-lab.de/index.html). Samples were filled into finger Schlenks in an Ar-filled glovebox and measured under Ar. FTIR spectra were collected on a Bruker Alpha FTIR instrument in the ATR geometry with a diamond ATR unit in the range 400–4000 cm-1 inside a LABStar MB 10 compact MBraun glove-box (argon atmosphere). (TEM-)EDX spectra for the composition determination of sample 4a-4c were recorded on a Tecnai G2 F20 equipped with a Schottky field emission gun operated at an acceleration voltage of 200 kV at the department of Mechanical Engineering, Ruhr-University Bochum. Liquid phase 1H-NMR spectra were measured on a Bruker Avance DPX-200 spectrometer at 293 K in DCl/DMSO-d6 for the digested activated MOF samples. CO adsorption (298 K) and the majority of N2 (99.999%) sorption (77 K) measurements were performed using a Micromeritics 3Flex instrument. The N2 sorption isotherms of 3a-3d were collected using a Quantachrome Autosorp-1 MP instrument, optimized protocols and N2 of 99.9995 % purity. Experiments on sorption of CO2 (298 K) and H2 (77 K) were conducted on a Micromeritics ASAP 2020 gas adsorption analyzer. The thermogravimetric analyses (TGA) were collected using a TG/DSC NETZSCH STA 409 PC instrument at a heating rate of 5 K min-1 in a temperature range from 30–600 °C at atmospheric pressure (sample weight 5–10 mg, N2 (99.999%;) gas flow (20 ml min-1). XANES spectra were recorded at the Ru-K edge (22117 eV) using a Si (311) monochromator at Beamline BL8 of the synchrotron radiation facility DELTA, TU Dortmund. The samples were filled into 1 mm caplillaries in an inert Ar atmosphere glovebox before the measurement. The XANES measurements were acquired using 15cm Ionchamber filled with Ar as I0, a 15 cm Ionchamber filled with Xe as I1 and a 30 cm Ionchamber filled with Xe as I2. Approx 30 mm above the sample was the PIN-Diode capturing a relatively wide solid angle of fluorescence radiation. The energy was calibrated by measuring a metallic Ru foil as reference simultaneously to each sample scan. The data processing and analysis were done using the program ATHENA.[32] Ultra High Vacuum (UHV) FT-IR measurements were performed using a novel UHV-FTIRS apparatus. The powder samples were first pressed into a stainless steel grid covered by gold and then mounted on a sample holder, which was specially designed for the FTIR transmission measurements under UHV conditions. The grid was cleaned by heating up to 850 K to remove all contaminants formed on it during preparation. The base pressure in the measurement chamber was 2 x 10-10 mbar. The optical path inside the IR spectrometer and the space between the spectrometer and UHV chamber were also evacuated to avoid atmospheric moisture adsorption resulting in a high sensitivity and stability. The MOF samples were cleaned in the UHV chamber by heating to 500 K in order to remove the contaminants involved during synthesis and all the adsorbed species such as water and hydroxyl groups. Prior to each exposure, a spectrum of the clean sample was recorded to be as a background reference. The exposure of the sample to CO and CO2 was carried out by backfilling the measurement chamber through a leak valve. All UHV-FTIR spectra were collected with 1024 scans at a resolution of 4 cm-1 in transmission mode. X-ray photoelectron spectroscopy (XPS) measurements were performed in a UHV setup equipped with a high-resolution Gammadata-Scienta SES 2002 analyzer. A monochromatic Al Kα X-ray source (energy 1486.6 eV) was used as incident radiation. The analyzer slit width was set at 0.3 mm and the pass energy was fixed at 200 eV for all the measurements. The overall energy resolution was better than 0.5 eV. A flood gun was used to compensate for the charging effects. All spectra reported here are calibrated to the C 1s corelevel binding energy at 285 eV. The XP spectra were deconvoluted using the CASA XPS program with a mixed Gaussian−Lorentzian function and Shirley background subtraction. Gas Chromatography measurements for Paal-Knorr reaction were performed on an Agilent Technologies 7890A with FID (Flame Ionization Detector) using a capillary column HP-5 (5% phenylmethylpolysiloxane) of 30 m length and 0.32 mm internal diameter as well as BP20(WAX)

of 15 m length and 0.32 mm internal diameter as another column. Thereby, the samples were measured in high dilution using volatile organic solvents (usually ethanol or acetone).

Synthesis of Ru-DEMOF samples (1a-1d, 2a-2d, 3a-3d, 4a-4c)

[Ru3(btc)2-x(5-X-ip)xYy]n (Y = counter ion; $0.1 \leq x \leq 1$; $0 \leq y \leq 1.5$). The samples were synthesized according to the reported method[19] applying the so-called controlled SBU approach. The mixtures of parent linker (1,3,5-benzenetricarboxylic acid, i.e. H3btc) and defective linker (5-X-isophthalic acid, i.e. 5-X-ipH2, X = OH (1), H (2), NH2 (3) and Br (4), respectively) combined with 1.5 molar equivalents of [Ru2(OOCCH3)4Cl]n (0.36 mmol,170 mg) were placed in the 20 ml Teflon vessels. Subsequently, 4 ml of HPLC grade water and 0.7 ml of glacial acetic acid were added. The molar ratios and amounts of the linkers used in the starting materials are listed in the Table S1. The Teflon reaction vessels were then placed in the Teflon-lined stainless steel autoclaves. The autoclaves were further sealed and placed into the pre-heated oven at 433 K for 72 h. Afterwards the autoclaves were taken out and cooled down at room temperature. The resulting powder products were collected by centrifugation. Afterwards, they were soaked into HPLC grade water (ca. 20 ml) and the solvent was refreshed by the same water amount every 24 hours for 3 times. Finally, the solvent was removed and collected powders were dried under air at room temperature. The activation of the solids was performed by heating at 423 K for 24 h under dynamic vacuum (ca. 10-3 mbar).

Catalytic reactions

1. Ethylene dimerization

In a typical run (entry 5), 2.1 mg of the activated Ru-MOF 1c was put in a 10 ml steel reactor followed by adding of 0.81 ml of Et2AlCl (1M in heptane), 2.1 ml of toluene and 0.09 ml of undecane (0.01 M in toluene). After degassing, the reactor was flushed with C2H4 (800psi) and placed in a pre-heated oil bath at 80 °C with stirring for 2 hours. Subsequently, the reaction was stopped and the reactor was cooled down at -7 °C in a mixture of dry ice and ethylene glycol bath. Cold distilled water was added to quench the reaction. The organic layer kept cold was then quickly analyzed by gas chromatography (SRI 8610V GC, 60 m x 0.54 mm internal diameter, 5.0 µm MXT-1 capillary columns) using undecane signal as a reference. For other entries, the amount of catalysts, the reaction temperature and time were varied and listed in Table S10. In case of no additive, the volume of toluene was changed to 2.91 ml. Other parameters are the same as entry 5 described above.

2. Paal-Knorr reaction

In a typical run, 5 mg of the activated Ru-MOF/DEMOFs in 0.5 ml of toluene were introduced into 125 mg (1.1 mmol) of 2,5-hexadione and 95 mg (1 mmol) of phenylamine and were stirred at 90 °C for 24h under air. The reaction was followed by taking aliquots every hour and analyzing the products by GC-MS. The reactions were performed in closed (pressurized) reaction vials.

Acknowledgements

This research was partially supported by the DFG project FI-502/32-1. W.Z. thanks for a PhD fellowship from the China Scholarship Council (CSC). W.Z is also grateful to the Research SchoolPlus at Ruhr-University Bochum for the support of her PhD project and funding of an internship at UC Berkeley at the group of Prof. J. R. Long and collaboration with D.J.X and M.G including Douglas Reed for the collection of CO isotherms (298K). W.Z. also thanks Dr. Raghavender Medishetty for the fruitful discussions. P.G. acknowledges the support of the EU

innovative Training Network “DEFect NETwork materials science and engineering” (DEFNET). The authors further thank the team at DELTA synchrotron facility at the TU Dortmund for the support with the X-ray absorption spectroscopy experiments performed at beam lines BL8 and the PXRD data collection at beam lines BL9.

Keywords: metal-organic frameworks • structural defects • ruthenium • sorption • heterogeneous catalysis

[1] a) M. Latroche, S. Surblé, C. Serre, C. Mellot-Draznieks, P. L. Llewellyn, J.-H. Lee, J.-S. Chang, S. H. Jhung, G. Férey, Angew. Chem. Int. Ed. 2006, 45, 8227-8231; b) X. Lin, J. Jia, X. Zhao, K. M. Thomas, A. J. Blake, G. S. Walker, N. R. Champness, P. Hubberstey, M. Schröder, Angew. Chem. Int. Ed. 2006, 45, 7358-7364; c) K. Sumida, D. L. Rogow, J. A. Mason, T. M. McDonald, E. D. Bloch, Z. R. Herm, T.-H. Bae, J. R. Long, Chem. Rev. 2012, 112, 724-781.

[2] a) A. Schneemann, E. D. Bloch, S. Henke, P. L. Llewellyn, J. R. Long, R. A. Fischer, Chem. Eur. J. 2015, 21, 18764-18769; b) E. D. Bloch, M. R. Hudson, J. A. Mason, S. Chavan, V. Crocellà, J. D. Howe, K. Lee, A. L. Dzubak, W. L. Queen, J. M. Zadrozny, S. J. Geier, L.-C. Lin, L. Gagliardi, B. Smit, J. B. Neaton, S. Bordiga, C. M. Brown, J. R. Long, J. Am. Chem. Soc. 2014, 136, 10752-10761; c) E. D. Bloch, W. L. Queen, R. Krishna, J. M. Zadrozny, C. M. Brown, J. R. Long, Science 2012, 335, 1606-1610.

[3] a) J. S. Seo, D. Whang, H. Lee, S. I. Jun, J. Oh, Y. J. Jeon, K. Kim, Nature 2000, 404, 982-986; b) A. Corma, H. García, F. X. Llabrés i Xamena, Chem. Rev. 2010, 110, 4606-4655.

[4] E. Biemmi, C. Scherb, T. Bein, J. Am. Chem. Soc. 2007, 129, 8054-8055.

[5] P. Horcajada, C. Serre, M. Vallet-Regí, M. Sebban, F. Taulelle, G. Férey, Angew. Chem. Int. Ed. 2006, 45, 5974-5978.

[6] a) R. A. Beyerlein, C. Choi-Feng, J. B. Hall, B. J. Huggins, G. J. Ray, Top. Catal., 4, 27-42; b) C. Baerlocher, D. Xie, L. B. McCusker, S.-J. Hwang, I. Y. Chan, K. Ong, A. W. Burton, S. I. Zones, Nat. Mater. 2008, 7, 631-635; c) B. Bonelli, L. Forni, A. Aloise, J. B. Nagy, G. Fornasari, E. Garrone, A. Gedeon, G. Giordano, F. Trifirò, Micropor. Mesopor. Mat. 2007, 101, 153-160.

[7] Z. Fang, B. Bueken, D. E. De Vos, R. A. Fischer, Angew. Chem. Int. Ed. 2015, 54, 7234-7254.

[8] U. Ravon, M. Savonnet, S. Aguado, M. E. Domine, E. Janneau, D. Farrusseng, Micropor. Mesopor. Mat. 2010, 129, 319-329.

[9] F. Vermoortele, B. Bueken, G. Le Bars, B. Van de Voorde, M. Vandichel, K. Houthoofd, A. Vimont, M. Daturi, M. Waroquier, V. Van Speybroeck, C. Kirschhock, D. E. De Vos, J. Am. Chem. Soc. 2013, 135, 11465-11468.

[10] S. S. Y. Chui, S. M. F. Lo, J. P. H. Charmant, A. G. Orpen, I. D. Williams, Science 1999, 283, 1148-1150.

[11] a) M. Kramer, U. Schwarz, S. Kaskel, J. Mater. Chem. 2006, 16, 2245-2248; b) C. R. Wade, M. Dinca, Dalton Trans. 2012, 41, 7931-7938.

[12] L. J. Murray, M. Dinca, J. Yano, S. Chavan, S. Bordiga, C. M. Brown, J. R. Long, J. Am. Chem. Soc. 2010, 132, 7856-7857.

[13] P. Maniam, N. Stock, Inorg. Chem. 2011, 50, 5085-5097.

[14] a) O. Kozachuk, K. Yusenko, H. Noei, Y. Wang, S. Walleck, T. Glaser, R. A. Fischer, Chem. Commun. 2011, 47, 8509-8511; b) H. Noei, O. Kozachuk, S. Amirjalayer, S. Bureekaew, M. Kauer, R. Schmid, B. Marler, M. Muhler, R. A. Fischer, Y. Wang, J. Phys. Chem. C 2013, 117, 5658-5666.

[15] J. I. Feldblyum, M. Liu, D. W. Gidley, A. J. Matzger, J. Am. Chem. Soc. 2011, 133, 18257-18263.

[16] S. Marx, W. Kleist, A. Baiker, J. Catal. 2011, 281, 76-87.

[17] Z. Fang, J. P. Dürholt, M. Kauer, W. Zhang, C. Lochenie, B. Jee, B. Albada, N. Metzler-Nolte, A. Pöppl, B. Weber, M. Muhler, Y. Wang, R. Schmid, R. A. Fischer, J. Am. Chem. Soc. 2014, 136, 9627-9636.

[18] G. Barin, V. Krungleviciute, O. Gutov, J. T. Hupp, T. Yildirim, O. K. Farha, Inorg. Chem. 2014, 53, 6914-6919.

[19] O. Kozachuk, I. Luz, F. X. Llabrés i Xamena, H. Noei, M. Kauer, H. B. Albada, E. D. Bloch, B. Marler, Y. Wang, M. Muhler, R. A. Fischer, Angew. Chem. Int. Ed. 2014, 53, 7058-7062.

[20] F. Schröder, D. Esken, M. Cokoja, M. W. E. van den Berg, O. I. Lebedev, G. Van Tendeloo, B. Walaszek, G. Buntkowsky, H.-H. Limbach, B. Chaudret, R. A. Fischer, J. Am. Chem. Soc. 2008, 130, 6119-6130.

[21] E. A. Braude, F. C. Nachod, Editors, Determination of Organic Structures by Physical Methods, Academic Press, 1955.

[22] W. Zhang, O. Kozachuk, R. Medishetty, A. Schneemann, R. Wagner, K. Khaletskaya, K. Epp, R. A. Fischer, Eur. J. Inorg. Chem. 2015, 2015, 3913-3920.

[23] F. Genin, F. Quiles, A. Burneau, Phys. Chem. Chem. Phys. 2001, 3, 932-942.

[24] K. Nakamoto, in Infrared and Raman Spectra of Inorganic and Coordination Compounds, John Wiley & Sons, Inc., 2008, pp. 1-273.

[25] K. S. W. Sing, D. H. Everett, R. A. W. Haul, L. Moscou, R. A. Pierotti, J. Rouquerol, T. Siemieniewska, Pure Appl. Chem. 1985, 57, 603-619.

[26] a) S. T. Madrahimov, J. R. Gallagher, G. Zhang, Z. Meinhart, S. J. Garibay, M. Delferro, J. T. Miller, O. K. Farha, J. T. Hupp, S. T. Nguyen, ACS catal. 2015, 5, 6713-6718; b) D. Yang, S. O. Odoh, J. Borycz, T. C. Wang, O. K. Farha, J. T. Hupp, C. J. Cramer, L. Gagliardi, B. C. Gates, ACS catal. 2016, 6, 235-247; c) J. Canivet, S. Aguado, Y. Schuurman, D. Farrusseng, J. Am. Chem. Soc. 2013, 135, 4195-4198; d) E. D. Metzger, C. K. Brozek, R. J. Comito, M. Dincă, ACS Cent. Sci. 2016.

[27] a) I. Ogino, B. C. Gates, Chem. Eur. J. 2009, 15, 6827-6837; b) I. Ogino, B. C. Gates, J. Am. Chem. Soc. 2008, 130, 13338-13346; c) G. Laurenczy, A. E. Merbach, J. Chem. Soc., Chem. Commun. 1993, 187-189.

[28] J. S. Bass, L. Kevan, J. Phys. Chem. 1990, 94, 1483-1489.

[29] a) A. L. Harreus, in Ullmann's Encyclopedia of Industrial Chemistry, Wiley-VCH Verlag GmbH & Co. KGaA, 2000; b) R. J. Sundberg, in Comprehensive Heterocyclic Chemistry II (Ed.: Scriven), Pergamon, Oxford, 1996, pp. 119-206.

[30] R. W. Mitchell, A. Spencer, G. Wilkinson, J. Chem. Soc., Dalton Trans. 1973, 846-854.

[31] A. P. Hammersley, S. O. Svensson, M. Hanfland, A. N. Fitch, D. Hausermann, High Pressure Res. 1996, 14, 235-248.

[32] B. Ravel, M. Newville, J. Synchrotron Radiat. 2005, 12, 537-541.

Entry for the Table of Contents (Please choose one layout)

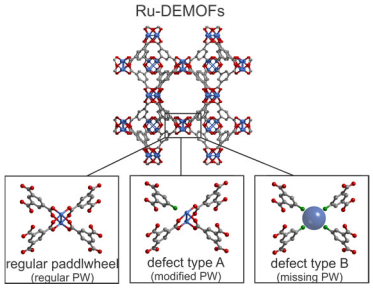

Employing mixed component solid solution approach, various 5-X-isophthalate linkers have been introduced into the Ru-analog of HKUST-1 to yield the isoreticular, defect-engineered Ru-MOFs. The characterization data are consistent with two kinds of defects (type A: modified paddlewheels and type B: missing paddlewheels) and their relative abundance is controlled by nature of the functional X-group of the defect generating linkers. Porosity, sorption and reactive properties correlate with the proposed defect structure.